ARTICLE

doi:10.1038/nature09913

Crystal structure of oxygen-evolving photosystem II at a resolution of 1.9 Å

Yasufumi Umena[1]†*, Keisuke Kawakami[2]†*, Jian-Ren Shen[2] & Nobuo Kamiya[1]†

Photosystem II is the site of photosynthetic water oxidation and contains 20 subunits with a total molecular mass of 350 kDa. The structure of photosystem II has been reported at resolutions from 3.8 to 2.9 Å. These resolutions have provided much information on the arrangement of protein subunits and cofactors but are insufficient to reveal the detailed structure of the catalytic centre of water splitting. Here we report the crystal structure of photosystem II at a resolution of 1.9 Å. From our electron density map, we located all of the metal atoms of the Mn_4CaO_5 cluster, together with all of their ligands. We found that five oxygen atoms served as oxo bridges linking the five metal atoms, and that four water molecules were bound to the Mn_4CaO_5 cluster; some of them may therefore serve as substrates for dioxygen formation. We identified more than 1,300 water molecules in each photosystem II monomer. Some of them formed extensive hydrogen-bonding networks that may serve as channels for protons, water or oxygen molecules. The determination of the high-resolution structure of photosystem II will allow us to analyse and understand its functions in great detail.

Photosystem II (PSII) is a membrane protein complex located in the thylakoid membranes of oxygenic photosynthetic organisms, and performs a series of light-induced electron transfer reactions leading to the splitting of water into protons and molecular oxygen. The products of PSII, namely chemical energy and oxygen, are indispensable for sustaining life on Earth. PSII from cyanobacteria is composed of 17 transmembrane subunits, three peripheral proteins and a number of cofactors, with a total molecular weight of 350 kDa. The light-induced oxidation of water is catalysed by a Mn_4Ca cluster that cycles through several different redox states (S_i, $i = 0$–4) on extraction of each electron by the PSII reaction centre, P_{680}[1,2]. When four electrons and four protons are extracted from two molecules of water, one molecule of dioxygen is formed. The structure of PSII has been solved at resolutions from 3.8 to 2.9 Å in two closely related thermophilic cyanobacteria, *Thermosynechococcus elongatus*[3–5] and *Thermosynechococcus vulcanus*[6]. These structural studies provided the arrangement of all of the protein subunits and the locations of chlorophylls and other cofactors, and formed a basis for further investigations into the functions of PSII. However, the resolution achieved so far is not high enough to reveal the structure of the Mn_4Ca cluster, the locations of substrate water molecules, or the precise arrangement of the amino-acid side chains and cofactors that may have significant mechanistic consequences for the energy, electron and proton transfer reactions. We have improved the resolution of the PSII crystals from *T. vulcanus* to 1.9 Å and analysed their structure (Methods, Supplementary Fig. 1 and Supplementary Table 1). This analysis provides many more details of the structure and of the coordination environments of the Mn_4Ca cluster and other cofactors than were previously available, and reveals the presence of a vast number of water molecules; these results may greatly advance our understanding of the energy, electron, proton transfer and water-splitting reactions taking place in PSII.

Overall structure

The overall structure is shown in Fig. 1. Every PSII monomer contains 19 protein subunits, among which PsbY was not found, suggesting that this subunit has been lost during purification or crystallization, presumably owing to its loose association with PSII[4–8]. The Cα superposition of our PSII dimer with the structure reported at a resolution of 2.9 Å (ref. 5) yielded a root mean square deviation of 0.78 Å, indicating that the overall structure determined at the lower resolution is well preserved in the present structure.

In addition to the protein subunits, there were 35 chlorophylls, two pheophytins, 11 β-carotenes, more than 20 lipids, two plastoquinones, two haem irons, one non-haem iron, four manganese atoms, three or four calcium atoms (one of which is in the Mn_4Ca cluster), three Cl^- ions (two of which are in the vicinity of the Mn_4Ca cluster), one bicarbonate ion and more than 15 detergents in a monomer (Supplementary Table 2). Within each PSII monomer, more than 1,300 water molecules were found, yielding a total of 2,795 water molecules in the dimer (Fig. 1a and Supplementary Table 1). As shown in Fig. 1b, the water molecules were organized into two layers located on the surfaces of the stromal and lumenal sides, respectively, with the latter having more water molecules than the former. A few water molecules were found within the membrane region, most of them serving as ligands to chlorophylls (see below). In the following, we describe the detailed structure and functions of the Mn_4CaO_5 cluster, as well as other cofactors, mainly on the basis of the structure of one of the two monomers, monomer A (chains labelled with capital letters in the accompanying Protein Data Bank file). There were some slight structural differences between the two monomers within the dimer; however, most of them are not related to the critical functions of PSII.

Structure of the Mn_4CaO_5 cluster

The electron densities of the four manganese atoms and the single calcium atom in the oxygen-evolving complex were well defined and clearly resolved, and the electron density for the calcium atom was lower than those of the manganese atoms, allowing us to identify the individual atoms unambiguously[4,5] (Fig. 2a). In addition, five oxygen

[1]Department of Chemistry, Graduate School of Science, Osaka City University, 3-3-138 Sugimoto, Sumiyoshi, Osaka 558-8585, Japan. [2]Division of Bioscience, Graduate School of Natural Science and Technology/Faculty of Science; Okayama University, Okayama 700-8530, Japan. †Present addresses: Institute for Protein Research, Osaka University, Suita, Osaka 565-0871, Japan (Y.U.); Department of Chemistry, Graduate School of Science, Osaka City University, 3-3-138 Sugimoto, Sumiyoshi, Osaka 558-8585, Japan (K.K.); The OCU Advanced Research Institute for Natural Science and Technology (OCARINA), Osaka City University, 3-3-138 Sugimoto, Sumiyoshi, Osaka 558-8585, Japan (N.K.).
*These authors contributed equally to this work.

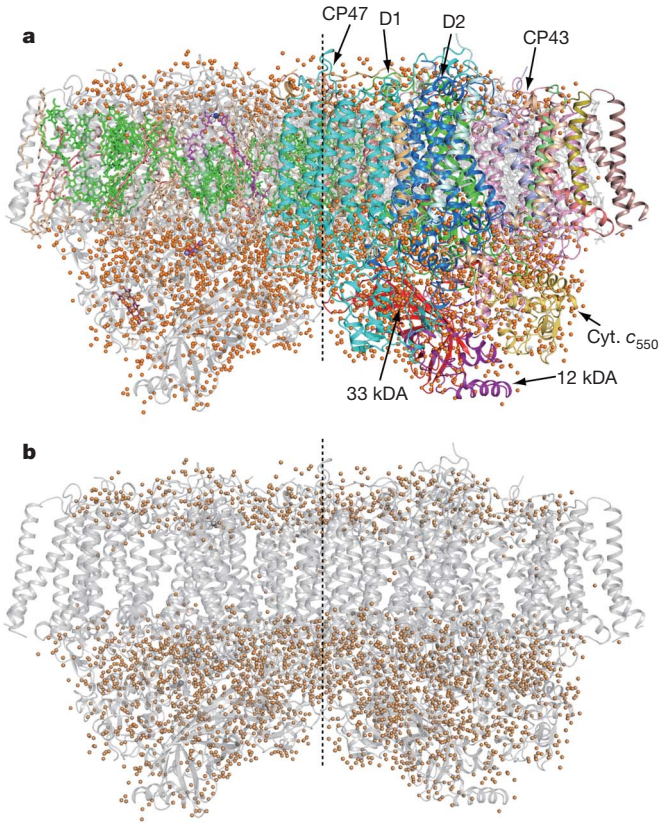

Figure 1 | Overall structure of PSII dimer from *T. vulcanus* at a resolution of 1.9 Å. View from the direction perpendicular to the membrane normal. **a**, Overall structure. The protein subunits are coloured individually in the right-hand monomer and in light grey in the left-hand monomer, and the cofactors are coloured in the left-hand monomer and in light grey in the right-hand monomer. Orange balls represent water molecules. **b**, Arrangement of water molecules in the PSII dimer. The protein subunits are coloured in light grey and all other cofactors are omitted. The central broken lines are the non-crystallographic two-fold axes relating the two monomers.

atoms were found to serve as oxo bridges linking the five metal atoms from the omit map (Fig. 2a). This gives rise to a Mn_4CaO_5 cluster. Of these five metals and five oxygen atoms, three manganese, one calcium and four oxygen atoms form a cubane-like structure in which the calcium and manganese atoms occupy four corners and the oxygen atoms occupy the other four. The bond lengths between the oxygens and the calcium in the cubane are generally in the range of 2.4–2.5 Å, and those between the oxygens and manganeses are in the range of 1.8–2.1 Å (Fig. 2b). However, the bond length between one of the oxygens at the corner of the cubane (O5) and the calcium is 2.7 Å, and those between O5 and the manganeses are in the range of 2.4–2.6 Å. Owing to these differences in bond lengths, the Mn_3CaO_4 cubane is not an ideal, symmetric one.

The fourth manganese (Mn4) is located outside the cubane and is linked to two manganeses (Mn1 and Mn3) within the cubane by O5 and the fifth oxygen (O4) by a di-μ-oxo bridge. In this way, every two adjacent manganeses are linked by di-μ-oxo bridges: Mn1 and Mn2 are linked by a di-μ-oxo bridge via O1 and O3, Mn2 and Mn3 are linked via O2 and O3, and Mn3 and Mn4 are linked via O4 and O5. The calcium is linked to all four manganeses by oxo bridges: to Mn1 via the di-μ-oxo bridge formed by O1 and O5, to Mn2 via O1 and O2, to Mn3 via O2 and O5, and to Mn4 via the mono-μ-oxo bridge formed by O5. The whole structure of the Mn_4CaO_5 cluster resembles a distorted chair, with the asymmetric cubane serving as the seat base and the isolated Mn4 and O4 serving as the back of the chair. The cubane-like structure has been reported previously[4,9–12], but the oxo bridges and exact distances among the individual atoms could not be determined at the medium resolution achieved previously[4].

The distances among the four manganeses determined for monomer A are 2.8 Å (Mn1–Mn2), 2.9 Å (Mn2–Mn3), 3.0 Å (Mn3–Mn4; 2.9 Å for monomer B), 3.3 Å (Mn1–Mn3) and 5.0 Å (Mn1–Mn4) (Fig. 2c). The distances between the calcium and the four manganeses are 3.5 Å (Ca–Mn1), 3.3 Å (Ca–Mn2), 3.4 Å (Ca–Mn3) and 3.8 Å (Ca–Mn4) (Fig. 2d; for the corresponding distances in monomer B and the average distances between the two monomers, see Supplementary Table 3). These distances are largely different from those reported in the previous crystal structures[3–6]; however, they are comparable to those reported from extended X-ray absorption fine structure studies[13,14] if we consider that there is an error of 0.16 Å in the distances determined from the X-ray structural analysis (Methods).

In addition to the five oxygens, four water molecules (W1 to W4) were found to be associated with the Mn_4CaO_5 cluster, of which W1 and W2 are coordinated to Mn4 with respective distances of 2.1 and 2.2 Å, and W3 and W4 are coordinated to the calcium with a distance of 2.4 Å. No other water molecules were found to associate with the other three manganeses, suggesting that some of the four waters may serve as the substrates for water oxidation.

All of the amino-acid residues coordinated to the Mn_4CaO_5 cluster were identified (Fig. 2e and Supplementary Table 4). Of these, D1-Glu 189 (D1 is one of the reaction centre subunits of PSII), served as a monodentate ligand to Mn1, which contradicts a previous report showing that it serves as a bidentate ligand[5]. All of the remaining five carboxylate residues served as bidentate ligands: D1-Asp 170 as a ligand to Mn4 and Ca, D1-Glu 333 to Mn3 and Mn4, D1-Asp 342 to Mn1 and Mn2, D1-Ala 344 (the carboxy-terminal residue of D1) to Mn2 and Ca, and CP43-Glu 354 to Mn2 and Mn3 (CP43 is one of the core antenna subunits of PSII). In addition, D1-His 332 is coordinated to Mn1, whereas D1-His 337 is not directly coordinated to the metal cluster. Most of the distances of the ligands to manganeses are in the range of 2.0–2.3 Å; the two shortest distances are 1.9 Å, between D1-Glu 189 and Mn1, and 2.0 Å, between D1-Ala 344 and Mn2 (Supplementary Table 3). The distances of two carboxylate ligands to the calcium, D1-Asp 170 and D1-Ala 344, are slightly longer (2.3–2.4 Å) than the ligand distances to the manganeses (Supplementary Table 3). Combining with the oxo bridges and waters, these give rise to a saturating ligand environment for the Mn_4CaO_5 cluster: each of the four manganeses has six ligands whereas the calcium has seven ligands (Supplementary Table 4). The ligation pattern and the geometric positions of the metal atoms revealed in the present structure may have important consequences for the mechanisms of water splitting and O–O bond formation.

In addition to the direct ligands of the Mn_4CaO_5 cluster, we found that D1-Asp 61, D1-His 337 and CP43-Arg 357 are located in the second coordination sphere and may have important roles in maintaining the structure of the metal cluster, in agreement with various reports showing the importance of these three residues in maintaining the oxygen-evolving activity[15–19]. One of the guanidinium η-nitrogens of CP43-Arg 357 is hydrogen-bonded to both O2 and O4 of the Mn_4CaO_5 cluster, whereas the other is hydrogen-bonded to the carboxylate oxygen of D1-Asp 170 and to that of D1-Ala 344. The imidazole ε-nitrogen of D1-His 337 is hydrogen-bonded to O3. These two residues may thus function to stabilize the cubane structure of the metal cluster as well as to provide partial positive charges to compensate for the negative charges induced by the oxo bridges and carboxylate ligands of the metal cluster. The carboxylate oxygen of D1-Asp 61 is hydrogen-bonded to W1, and also to O4 indirectly through another water molecule, suggesting that this residue may also contribute to stabilizing the metal cluster. Furthermore, D1-Asp 61 is located at the entrance of a proposed proton exit channel involving a chloride ion (Cl^-1; see below), suggesting that this residue may function in facilitating proton exit from the Mn_4CaO_5 cluster[5,20,21].

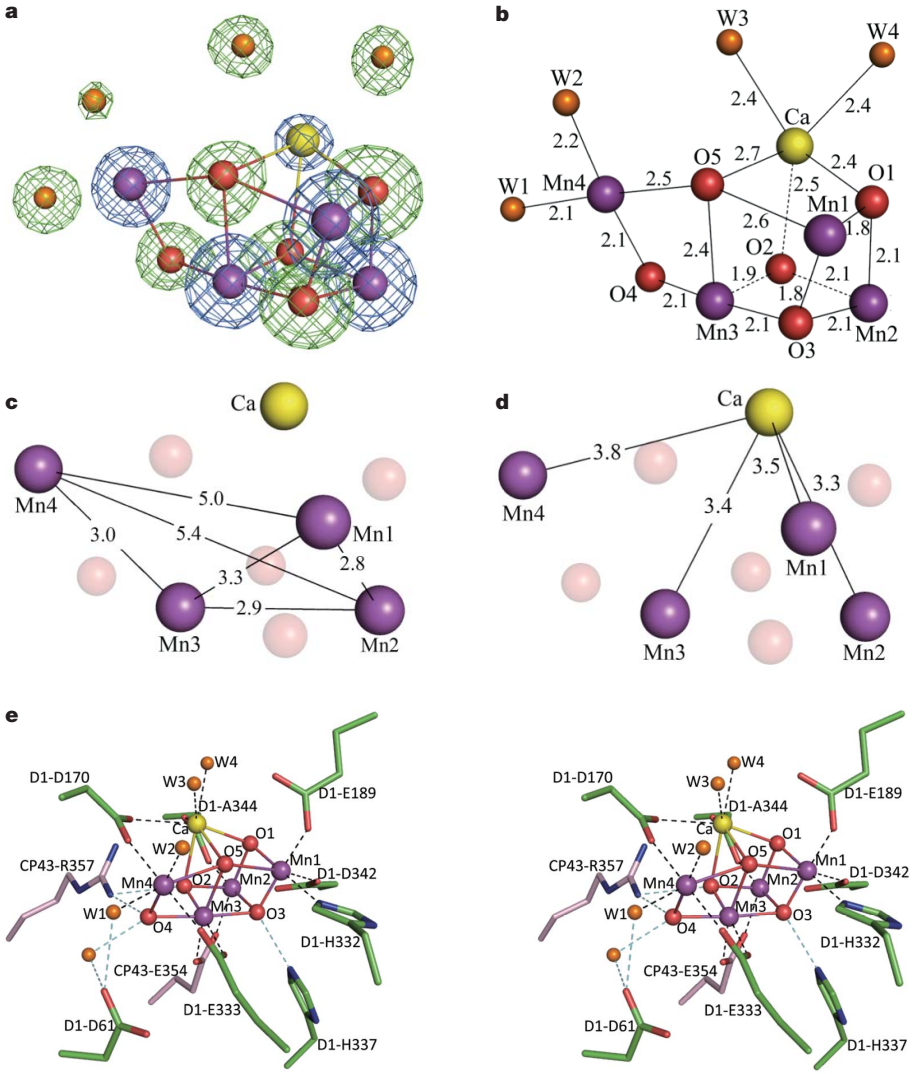

Figure 2 | Structure of the Mn_4CaO_5 cluster. **a**, Determination of individual atoms associated with the Mn_4CaO_5 cluster. The structure of the cluster was superimposed with the $2F_o - F_c$ map (blue) contoured at 5σ for manganese and calcium atoms, and with the omit map (green) contoured at 7σ for oxygen atoms and water molecules. **b**, Distances (in ångströms) between metal atoms and oxo bridges or water molecules. **c**, Distances between each pair of manganese atoms. **d**, Distances between the manganese and the calcium atoms. **e**, Stereo view of the Mn_4CaO_5 cluster and its ligand environment. The distances shown are the average distances between the two monomers. Manganese, purple; calcium, yellow; oxygen, red; D1, green; CP43, pink.

The most significant structural feature of the Mn_4CaO_5 cluster, which may be important for elucidating the mechanism of the water-splitting reaction, is its distorted chair form. The large distortion is principally caused by the existence of the calcium and O5 in the Mn_4CaO_5 cluster, as described above. The apparently longer distances between O5 and metal atoms suggested that the corresponding bonds are weak, and that O5 may therefore have a lower negative charge than the valence of −2 expected for normal oxygen atoms in oxo bridges. This in turn suggests that O5 may exist as a hydroxide ion in the S_1 state and may provide one of the substrates for dioxygen formation. Because both W2 and W3 are within the hydrogen-bond distances to O5, one of these two waters may provide another substrate.

Because the transition between S_0 and S_1 is fastest in the Kok cycle, the proton released during this transition may be accepted by D1-Tyr 161 (also termed Y_Z), which is deprotonated by means of proton-coupled electron transfer (PCET; see below). W3 is closer to Y_Z than is O5 (Fig. 3a) and may be a more favourable candidate than O5 as the proton-releasing group. Thus, W3 rather than O5 may be a hydroxide ion in the S_1 state, suggesting that O–O bond formation may occur between W2 and W3. In any case, our results suggest that the O–O bond formation occurs in two of the three species O5, W2 and W3.

Hydrogen-bond network around Y_Z

Y_Z is located between the Mn_4CaO_5 cluster and the PSII reaction centre, and functions to mediate electron transfer between the two. We found an extensive hydrogen-bonding network between Y_Z and the Mn_4CaO_5 cluster and from Y_Z to the lumenal bulk phase. Y_Z was hydrogen-bonded to the two waters coordinated to the calcium either directly (W4) or indirectly through another water (W3; Fig. 3a). The hydrogen bond between the additional water and Y_Z that mediates the link from W3 to Tyr161 has a length of 2.6 Å, suggesting that this is a strong (low-barrier) hydrogen bond[22]. This additional water also mediates the hydrogen bond between the two waters bound to Mn4 and Y_Z. Furthermore, another strong hydrogen bond was found between Y_Z and the ε-nitrogen of D1-His 190, which is 2.5 Å in length and lies on the opposite side of the Mn_4CaO_5 cluster. D1-His 190 was further hydrogen-bonded to D1-Asn 298 and to several waters and residues including CP43-Ala 411, D1-Asn 322 and PsbV-Tyr 137 (the C-terminal residue of the PsbV subunit), leading to an exit pathway to the lumenal bulk solution (Fig. 3b). This hydrogen-bond network is located in the interfaces between the D1, CP43 and PsbV subunits and may function as an exit channel for protons that arise from PCET via Y_Z. This provides support for the existence of a PCET pathway involving Y_Z

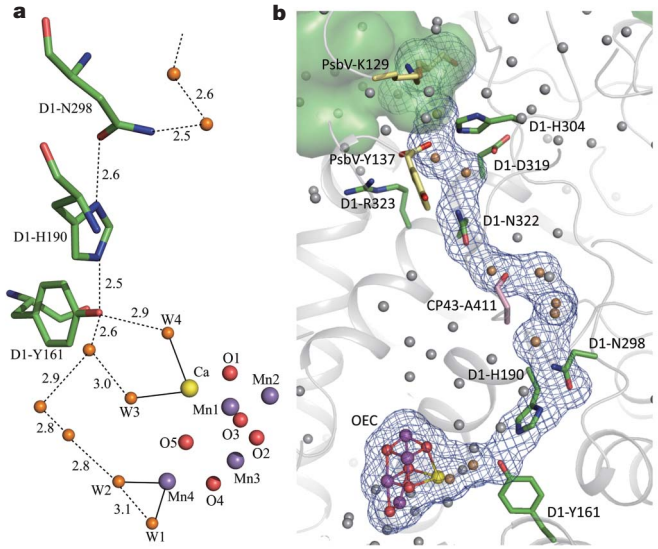

Figure 3 | Hydrogen-bond network around Y_Z. **a**, Hydrogen bonds around Y_Z (D1-Tyr 161). The bonds between metal atoms and water ligands are depicted as solid lines, and the hydrogen bonds are depicted as dashed lines. Distances are expressed in ångströms. **b**, Hydrogen-bond network from the Mn_4CaO_5 cluster through Y_Z to the lumenal bulk phase. Water molecules participating in the hydrogen-bond network are depicted in orange, whereas those not participating are depicted in grey. The area in green in the upper left corner represents the lumenal bulk surface. PsbV, pale yellow; other colour codes are the same as in Fig. 2. OEC, oxygen-evolving complex.

and D1-His 190, as implied by a number of previous studies[23–25]. PsbV-Tyr 137, at the exit of this channel, is surrounded by several charged residues including D1-Arg 323, D1-His 304 and PsbV-Lys 129; these residues may therefore function to regulate the proton excretion through the PCET pathway (Fig. 3b).

The other redox-active tyrosine residue, Y_D (D2-Tyr 160), has a different, rather hydrophobic, environment from that of Y_Z. For a discussion of the environment of Y_D, see Supplementary Fig. 3 and discussions.

The structure and function of chloride-binding sites

Previous studies have identified two chloride ions (Cl^-) in the vicinity of the Mn_4CaO_5 cluster by substitution of Br^- or I^- for Cl^- (refs 26, 27), although only one Cl^- site was visible in the native PSII crystals[5]. In the present study, the electron density for the two Cl^--binding sites were clearly visible (Fig. 4a), which were confirmed from the anomalous difference Fourier map calculated with data collected at a wavelength of 1.75 Å (Fig. 4a). The two Cl^--binding sites are located in the same position as those reported for Br^-- or I^--substituted PSII previously[26,27] (Fig. 4b, c). Both Cl^- ions are surrounded by four species, among which two are waters. For one of the ions, Cl^-1, the other two species are the amino group of D2-Lys 317 and the backbone nitrogen of D1-Glu 333, and for the other ion, Cl^-2, they are the backbone nitrogens of D1-Asn 338 and CP43-Glu 354. Because the side chains of D1-Glu 333 and CP43-Glu 354 are coordinated to the Mn_4CaO_5 cluster directly, the two Cl^- anions may function to maintain the coordination environment of the Mn_4CaO_5 cluster, thereby allowing the oxygen-evolving reaction to proceed properly.

In addition to the structural roles, the two Cl^--binding sites were found to lie at the entrance of hydrogen-bond networks starting from the Mn_4CaO_5 cluster and extending towards the lumenal bulk solution (Fig. 4b, c). The network through Cl^-1 was located in the interface of the D1, D2 and PsbO subunits, and that through Cl^-2 was located in the interface of the D1, CP43 and PsbU subunits. These hydrogen-bond networks involve a number of bound waters and some hydrophilic or charged amino-acid residues; they thus may function as either proton exit channels or water inlet channels.

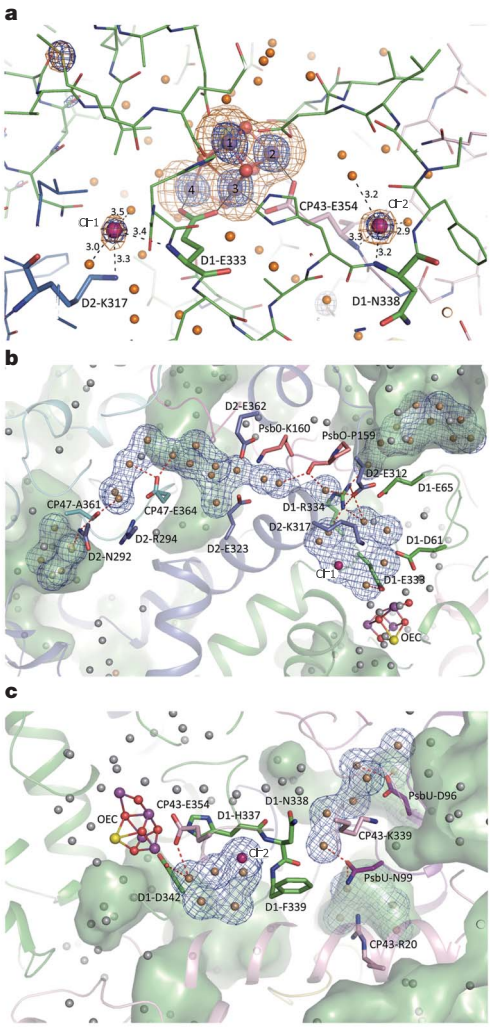

Figure 4 | Structure of two Cl^--binding sites. **a**, Location of the two Cl^- ions. Blue mesh, $2F_o - F_c$ map contoured at 4σ, measured at a wavelength of 0.9 Å; orange mesh, anomalous difference Fourier map contoured at 8σ, measured at a wavelength of 1.75 Å. The small density at the upper left corner is from the sulphur atom of D1-Met 328. Distances are expressed in ångströms. **b**, Hydrogen-bond network from the Mn_4CaO_5 cluster through the Cl^-1-binding site to the lumenal bulk phase. **c**, Hydrogen-bond network from the Mn_4CaO_5 cluster through the Cl^-2-binding site to the lumenal bulk phase. Colour codes are the same as in Figs 2 and 3.

Chlorophylls and β-carotenes

The positions and orientations of most chlorophylls are similar to those reported previously[4–6]. However, we determined the ligands to the central magnesium of all of chlorophylls, of which seven are coordinated by water instead of amino-acid residues (Fig. 5a and Supplementary Table 5). These are Chl6 (the accessory chlorophyll of D1); Chl7 (the accessory chlorophyll of D2); Chl12, Chl18 and Chl21, harboured by CP47; and Chl-31 and Chl-34, harboured by CP43. In addition, Chl38 was coordinated by CP43-Asn 39 and all other chlorophylls are coordinated by histidines. From our electron density map, we confirmed that all of the C8 and C13 positions in the phytol chains have a (*R*, *R*) configuration, in agreement with the stereochemistry determined for the complete phytol chain[28,29]. Furthermore, we found that most of the vinyl groups are located in or near the same plane of the tetrapyrrole ring, which may contribute to the extension of energy coupling within the plane and hence facilitate the energy migration between adjacent chlorophylls.

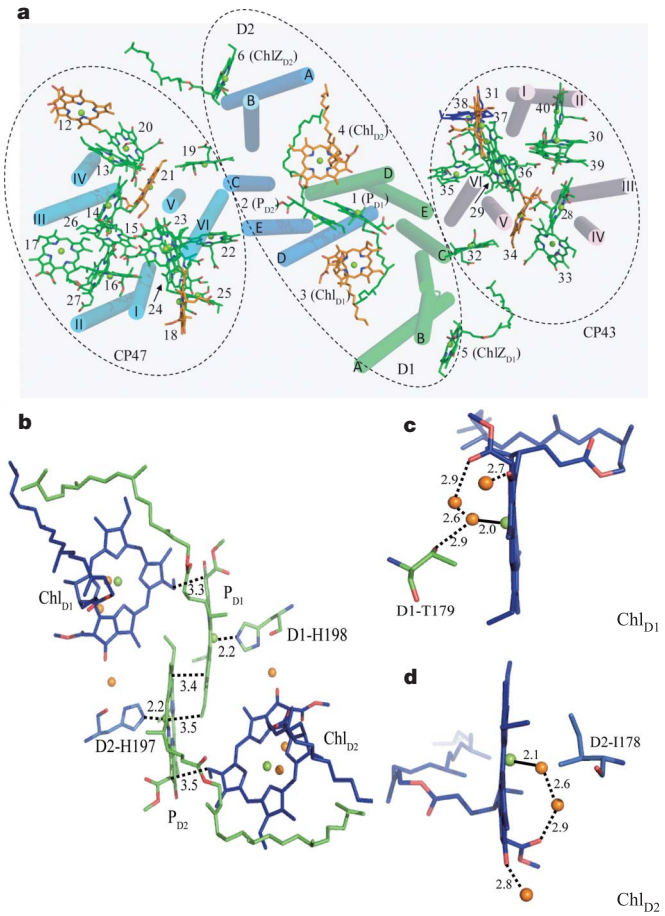

Figure 5 | Organization of chlorophylls. a, Organization of 35 chlorophylls in a PSII monomer. Chlorophylls (Chl) whose central magnesium atoms are coordinated by water are depicted in orange, and one chlorophyll coordinated by CP43-Asn 39 is depicted in blue. All other chlorophylls are coordinated by His and are depicted in green. Transmembrane helices of D1 and D2 are labelled A–E, and transmembrane helices of CP47 and CP43 are labelled I–VI. **b**, Organization of the four reaction-centre chlorophylls. Magnesium atoms of chlorophylls are depicted in green, and water molecules are depicted in orange. The edge-to-edge distances are expressed in ångströms. **c**, Water ligand and hydrogen bonds of Chl_{D1}. **d**, Water ligand and hydrogen bonds of Chl_{D2}.

The four chlorophylls constituting the PSII reaction centre are depicted in Fig. 5b. The non-crystallographic two-fold symmetry expected for the chlorophyll dimer comprising P_{D1} and P_{D2} seems to be broken in our high-resolution structure, as follows. The vinyl group of P_{D1} is roughly in plane, and its terminal carbon atom is close to the magnesium of P_{D2} at its sixth coordination site. In contrast, the corresponding vinyl group of P_{D2} is out of the chlorin plane and is located some distance from the magnesium of P_{D1}. The edge-to-edge distances that are able to form π–π stacking or CH–π stacking among the four chlorophylls range from 3.3 to 3.5 Å, with the shortest being 3.3 Å, between P_{D1} and Chl_{D1}. This may account partly for the preferential electron transfer along the D1 side. Importantly, although both water ligands to the two 'accessory chlorophylls' Chl_{D1} and Chl_{D2} are hydrogen-bonded to the carbonyl oxygen of the methoxycarbonyl group of chlorin ring V, the water ligand of Chl_{D1} is further hydrogen-bonded to D1-Thr 179 but no such a hydrogen-bond partner is found for Chl_{D2} (Fig. 5c, d). These discrepancies may also contribute to the functional differences between the two chlorophylls.

CP47 and CP43 bind 16 and 13 antenna chlorophylls, respectively, which are arranged as double layers connected by a special chlorophyll at the middle of the two layers[30]. The chlorophylls are distributed in one of three areas separated by coiled-coil helix dimers (I, II), (III, IV) and (V, VI) of CP47 (or CP43) (Fig. 5a, Supplementary Fig. 4 and Supplementary Discussions). A significant feature of the present structure is that the chlorin rings of most of the chlorophylls are not planar, which may affect the electronic, spectroscopic or energetic properties of the chlorophylls.

The positions and orientations of most of the β-carotenes are similar to those in the previous structures (Supplementary Fig. 5 and Supplementary Discussions). Each of the 11 β-carotenes was found to be of all-*trans* type.

Plastoquinones, non-haem iron and lipids

The two plastoquinones, Q_A and Q_B, were found in positions similar to those reported previously (Supplementary Fig. 5), with Q_B being less defined and having a higher B-factor than Q_A. Q_C, a third plastoquinone found in the previous structure[5], was not found in the present structure, probably as a result of the differences in preparation or crystallization conditions between the previous and present studies.

Six monogalactosyldiacylglycerol (MGDG), five digalactosyldiacylglycerol (DGDG), four sulfoquinovosyldiacylglycerol (SQDG) and five phosphatidylglycerol molecules were found (Supplementary Table 2, Supplementary Fig. 5 and Supplementary Discussions). All of the SQDGs and phosphatidylglycerols were distributed in the stromal side, with their head groups located in the stromal surface of the membrane, whereas all of the MGDGs and DGDGs, except for one MGDG, were located in the lumenal side. This may suggest that the hydrophilic head groups of SQDG and phosphatidylglycerol cannot penetrate the membrane, resulting in their preferential distribution in the stromal side, but that the more hydrophobic lipids MGDG and DGDG were able to transfer across the membrane.

For the structure of the non-haem iron and bicarbonate, see Supplementary Fig. 6 and Supplementary Discussions.

Conclusion

The high-resolution structure of PSII reveals the geometric arrangement of the Mn_4CaO_5 cluster as well as its oxo bridges and ligands, and four bound water molecules. This provides a basis for unravelling the mechanism of water splitting and O–O bond formation, one of nature's most fascinating and important reactions. In addition, our determination of the precise arrangement of amino-acid side chains and cofactors gives us a solid structural understanding of energy migration, electron transfer and water-splitting reactions taking place within PSII.

METHODS SUMMARY

We purified PSII core complexes highly active in oxygen evolution from a thermophilic cyanobacterium, *T. vulcanus*[31,32]. The homogeneity of PSII was improved by introducing a re-crystallization step. Previous crystallization conditions[6,32] were improved to produce high-resolution crystals (Methods). A typical diffraction pattern is shown in Supplementary Fig. 1, from which diffraction spots beyond a resolution of 1.8 Å could be observed. To suppress the possible radiation damage to a minimum level, we used a slide-oscillation method, resulting in the X-ray dose at each point of the crystal being lower than in previous experiments[33]. A full data set was collected at a wavelength of 0.9 Å and processed to a resolution of 1.9 Å (Supplementary Table 1). For identifying the positions of Cl^- ions, another data set was taken at a wavelength of 1.75 Å, and processed to a resolution of 2.5 Å.

The structure of PSII was solved by the molecular replacement method using the structure reported at a resolution of 2.9 Å as the search model[5] (Protein Data Bank ID, 3BZ1), and refined to R_{cryst} and R_{free} values of 0.174 and 0.201, respectively, with a Cruickshank diffraction-component precision index[34] of 0.11 Å. Detailed procedures for crystallization and structure determination can be found in Methods.

Full Methods and any associated references are available in the online version of the paper at www.nature.com/nature.

Received 1 December 2010; accepted 8 February 2011.
Published online 17 April 2011.

1. Kok, B., Forbush, B. & McGloin, M. Cooperation of charges in photosynthetic oxygen evolution. I. A linear four step mechanism. *Photochem. Photobiol.* **11,** 457–475 (1970).

2. Joliot, P. Period-four oscillations of the flash-induced oxygen formation in photosynthesis. *Photosynth. Res.* **76,** 65–72 (2003).
3. Zouni, A. *et al.* Crystal structure of photosystem II from *Synechococcus elongatus* at 3.8 Å resolution. *Nature* **409,** 739–743 (2001).
4. Ferreira, K. N., Iverson, T. M., Maghlaoui, K., Barber, J. & Iwata, S. Architecture of the photosynthetic oxygen-evolving center. *Science* **303,** 1831–1838 (2004).
5. Guskov, A. *et al.* Cyanobacterial photosystem II at 2.9 Å resolution and role of quinones, lipids, channels and chloride. *Nature Struct. Mol. Biol.* **16,** 334–342 (2009).
6. Kamiya, N. & Shen, J.-R. Crystal structure of oxygen-evolving photosystem II from *Thermosynechococcus vulcanus* at 3.7-Å resolution. *Proc. Natl Acad. Sci. USA* **100,** 98–103 (2003).
7. Kawakami, K., Iwai, M., Ikeuchi, M., Kamiya, N. & Shen, J.-R. Location of PsbY in oxygen-evolving photosystem II revealed by mutagenesis and X-ray crystallography. *FEBS Lett.* **581,** 4983–4987 (2007).
8. Broser, M. *et al.* Crystal structure of monomeric photosystem II from *Thermosynechococcus elongatus* at 3.6 Å resolution. *J. Biol. Chem.* **285,** 26255–26262 (2010).
9. De Paula, J. C., Beck, W. F. & Brudvig, G. W. Magnetic properties of manganese in the photosynthetic O_2-evolving complex. 2. Evidence for a manganese tetramer. *J. Am. Chem. Soc.* **108,** 4002–4009 (1986).
10. Carrell, G., Tyryshkin, A. M., &. Dismukes, G. C. An evaluation of structural models for the photosynthetic water-oxidizing complex derived from spectroscopic and X-ray diffraction signatures. *J. Biol. Inorg. Chem.* **7,** 2–22 (2002).
11. Vincent, J. B. & Christou, G. A molecular 'double-pivot' mechanism for water oxidation. *Inorg. Chim. Acta* **136,** L41–L43 (1987).
12. Peloquin, J. M. & Britt, R. D. EPR/ENDOR characterization of the physical and electronic structure of the OEC Mn cluster. *Biochim. Biophys. Acta* **1503,** 96–111 (2001).
13. Robblee, J. H., Cince, R. M. & Yachandra, V. K. X-ray spectroscopy-based structure of the Mn cluster and mechanism of photosynthetic oxygen evolution. *Biochim. Biophys. Acta* **1503,** 7–23 (2001).
14. Zein, S. *et al.* Focusing the view on nature's water-splitting catalyst. *Phil. Trans. R. Soc. B* **363,** 1167–1177 (2008).
15. Nixon, P. J. & Diner, B. Analysis of water-oxidation mutants constructed in the cyanobacterium *Synechocystis* sp. PCC 6803. *Biochem. Soc. Trans.* **22,** 338–343 (1994).
16. Chu, H.-A., Nguyne, A. P. & Debus, R. J. Amino acid residues that influence the binding of manganese or calcium to Photosystem II. 1. The lumenal inter-helical domains of the D1 polypeptide. *Biochemistry* **34,** 5839–5858 (1995).
17. Hwang, H. J., Dilbeck, P., Debus, R. J. & Burnap, R. L. Mutation of arginine 357 of the CP43 protein of photosystem II severely impairs the catalytic S-state cycle of the H_2O oxidation complex. *Biochemistry* **46,** 11987–11997 (2007).
18. Debus, R. J. Protein ligation of the photosynthetic oxygen-evolving center. *Coord. Chem. Rev.* **252,** 244–258 (2008).
19. Service, R. J., Hillier, W. & Debus, R. J. Evidence from FTIR difference spectroscopy of an extensive network of hydrogen bonds near the oxygen-evolving Mn_4Ca cluster of photosystem II involving D1-Glu65, D2-Glu312, and D1-Glu329. *Biochemistry* **49,** 6655–6669 (2010).
20. Murray, J. W. & Barber, J. Structural characteristics of channels and pathways in photosystem II including the identification of an oxygen channel. *J. Struct. Biol.* **159,** 228–237 (2007).
21. Ho, F. M. & Styring, S. Access channels and methanol binding site to the $CaMn_4$ cluster in Photosystem II based on solvent accessibility simulation, with implications for substrate water access. *Biochim. Biophys. Acta* **1777,** 140–153 (2008).
22. Zhang, C. Low-barrier hydrogen bond plays key role in active photosystem II—A new model for photosynthetic water oxidation. *Biochim. Biophys. Acta* **1767,** 493–499 (2007).
23. Hoganson, C. W. & Babcock, G. T. A metalloradical mechanism for the generation of oxygen from water in photosynthesis. *Science* **277,** 1953–1956 (1997).
24. Tommos, C. & Babcock, G. T. Proton and hydrogen currents in photosynthetic water oxidation. *Biochim. Biophys. Acta* **1458,** 199–219 (2000).
25. Hays, A.-M. A., Vassiliev, I. R., Golbeck, J. H. & Debus, R. J. Role of D1-His190 in the proton-coupled oxidation of tyrosine Y_Z in manganese-depleted photosystem II. *Biochemistry* **38,** 11851–11865 (1999).
26. Murray, J. W. *et al.* X-ray crystallography identifies two chloride binding sites in the oxygen evolving centre of photosystem II. *Energy Environ. Sci.* **1,** 161–166 (2008).
27. Kawakami, K., Umena, Y., Kamiya, N. & Shen, J.-R. Location of chloride and its possible functions in oxygen-evolving photosystem II revealed by X-ray crystallography. *Proc. Natl Acad. Sci. USA* **106,** 8567–8572 (2009).
28. Burrel, J. W. K., Jackman, L. M. & Weedon, B. L. C. Stereochemistry and synthesis of phytol, geraniol, and nerol. *Proc. Chem. Soc.* **1959,** 263–264 (1959).
29. Crabbe, P., Djerassi, C., Eisenbraun, E. J. & Liu, S. Optical rotatory dispersion studies. XXIX. Absolute configuration of phytol. *Proc. Chem. Soc.* **1959,** 264–265 (1959).
30. Vasil'ev, S., Orth, P., Zouni, A., Owens, T. G. & Bruce, D. Excited-state dynamics in photosystem II: Insights from the x-ray crystal structure. *Proc. Natl Acad. Sci. USA* **98,** 8602–8607 (2001).
31. Shen, J.-R. & Inoue, Y. Binding and functional properties of two new extrinsic components, cytochrome c-550 and a 12 kDa protein, in cyanobacterial photosystem II. *Biochemistry* **32,** 1825–1832 (1993).
32. Shen, J.-R. & Kamiya, N. Crystallization and the crystal properties of the oxygen-evolving photosystem II from *Synechococcus vulcanus*. *Biochemistry* **39,** 14739–14744 (2000).
33. Yano, J. *et al.* X-ray damage to the Mn_4Ca complex in single crystals of photosystem II: a case study for metalloprotein crystallography. *Proc. Natl Acad. Sci. USA* **102,** 12047–12052 (2005).
34. Cruickshank, D. W. J. Remarks about protein structure precision. *Acta Crystallogr. D* **55,** 583–601 (1999).

Supplementary Information is linked to the online version of the paper at www.nature.com/nature.

Acknowledgements The X-ray diffraction data was taken at beamlines BL44XU, BL41XU and BL38B1 at SPring-8. We thank E. Yamashita, N. Shimizu, S. Baba and N. Mizuno for their help in using the beamlines. J.-R.S. thanks Y. Inoue for his support in the initiation of this work. This work was supported by a Grant-in-Aid for Scientific Research on Priority Areas (Structures of Biological Macromolecular Assemblies), a Grant-in-Aid for Creative Scientific Research, a GCOE programme on Pico-biology at the University of Hyogo, a Grant-in-Aid for Scientific Research (C), from the Ministry of Education, Culture, Sports, Science and Technology of Japan, and a research grant from the Yamada Science foundation.

Author Contributions K.K. performed, and J.-R.S. supervised, the purification and crystallization of PSII. K.K., Y.U. and J.-R.S. performed X-ray diffraction experiments. Y.U. analysed the structure, and N.K. supervised the structure analysis and refinement process. J.-R.S. and N.K. jointly wrote the paper, and all of the authors joined the discussion of the results.

Author Information Atomic coordinates have been deposited in the Protein Data Bank under the accession number 3ARC. Reprints and permissions information is available at www.nature.com/reprints. The authors declare no competing financial interests. Readers are welcome to comment on the online version of this article at www.nature.com/nature. Correspondence and requests for materials should be addressed to J.-R.S. (shen@cc.okayama-u.ac.jp) and N.K. (nkamiya@sci.osaka-cu.ac.jp).

METHODS

Purification and crystallization. Highly active, dimeric PSII was purified from the thermophilic cyanobacterium *T. vulcanus* following refs 31, 32, and the crystals were grown as described previously[6,32]. To improve the crystal quality, the purity and homogeneity of PSII was improved by introducing a re-crystallization step in which the PSII core complexes were first crystallized in 12–24 h on ice or at 4 °C, and the microcrystals obtained were collected, re-solubilized and used for the second crystallization step. Sometimes the re-crystallization step was repeated to ensure a higher homogeneity of the samples, which were monitored by dynamic light-scattering measurements. The re-crystallization procedure typically decreased the polydispersity of the samples from 30% to around 20%.

The PSII crystals obtained were subjected to a post-crystallization dehydration procedure by increasing the concentrations of glycerol and PEG in the following way. The crystals were first transferred into a 150-μl buffer solution containing 6% PEG 3000 in place of 4–5% PEG 1450 in the original crystallization buffer concentrations (which contained no glycerol). After 25–30 min of incubation at 12 °C, half of the buffer volume was replaced with a new buffer containing a 1.4%-higher concentration of PEG 3000 and an additional 2.5% glycerol. This procedure was repeated every 25–30 min until the concentrations of glycerol and PEG 3000 reached 25% and 20%, respectively, in the final buffer. The crystals were then dehydrated by evaporation against air with a humidity of 75–90% in the final buffer for 2.5 h in the incubator at 12 °C, frozen in flash-cooling nitrogen gas and stored in liquid nitrogen. The crystals thus obtained had an approximate water content of 57%, which is much lower than both that of the crystals obtained previously[32] (66%) and that of the crystals used to analyse the structure at a resolution of 2.9 Å (ref. 5; 61%). All of the cryoprotectant replacement and cryocooling procedures were carried out under dim green light to avoid possible advancement of the S-states in the Kok cycle. A typical diffraction pattern of the PSII crystals is shown in Supplementary Fig. 1, in which diffraction spots beyond a resolution of 1.8 Å can be observed.

Data collection. After dehydration, the crystals were coated with a mixture of oil containing 66.5% Paratone-N, 28.5% paraffin oil and 5% glycerol, and flash-cooled at 100 K with a nitrogen gas stream. Two diffraction data sets were collected from two PSII crystals, one with a wavelength of 0.9 Å and the other one with a wavelength of 1.75 Å, at beamline BL44XU of SPring-8 (Japan). The X-ray beam had a size of $50 \times 50\ \mu m^2$, and the diffraction images were recorded with a Mar225HE charge-coupled-device detector. For the data set taken at 0.9 Å, we used a large PSII crystal with a size of $0.2 \times 0.7 \times 1.0\ mm^3$. The crystal was shifted by 30 μm to an adjacent point along the oscillation axis after recording 100 oscillation images, each of which was rotated by 0.2° relative to the last. Each point therefore covered a range of 20°. We collected a total of 900 images from nine irradiation points, covering a rotation angle of 180°. The data were processed and scaled using XDS and XSCALE[35] (Supplementary Table 1).

The photon flux of the beamline used (BL44XU) was 0.7×10^{11} photons s^{-1} (with an attenuator of 0.2-mm aluminium), and the exposure time was 1 s for each diffraction image. This gave rise to a total X-ray dose of 2.5×10^{10} photons μm^{-2} for the total of 900 images. Because the whole data set was divided into nine spots on the crystal, each spot received a total dose of 0.28×10^{10} photons μm^{-2}. If we consider that each point was rotated by 20° during data collection, the X-ray dose on a unit volume of the crystal will be slightly lower. This dose is much lower than that used previously[3–6], and is also at a low level of the dose range reported to induce possible radiation damage in the Mn_4CaO_5 cluster[33].

For the data set taken at a wavelength of 1.75 Å, we collected 2,400 oscillation images, each rotated by 0.3° over a range of 360°. For each of the data wedges of 10°, an inverse beam geometry was used to measure the Friedel pairs directly. The data was processed with HKL2000[36], and the reflection data statistics are summarized in Supplementary Table 1.

Structure refinement. An initial structure of the PSII dimer was obtained with the molecular replacement method of CNS[37] using the structure of PSII monomer[5] (PDB ID, 3BZ1) as a search model. The first stage of structure refinement was carried out using the CNS program package and the second stage was performed with REFMAC5 in the CCP4 program suite[38]. The two monomers in the PSII dimer were refined separately, and the structural model was revised using COOT[39]. Structures of cofactors, lipids, detergents and water molecules were determined and refined as described below. The refinement statistics are presented in Supplementary Table 1.

Mn_4CaO_5 cluster. The locations of the metal atoms of the Mn_4CaO_5 cluster, namely four manganese atoms and one calcium atom, were determined using a composite omit $2F_o - F_c$ map. Oxygen atoms forming oxo bridges in the Mn_4Ca cluster were identified and determined with an $F_o - F_c$ omit map. The electron density of the O5 atom in the Mn_4CaO_5 cluster was affected heavily by electron density distributions of the nearby metal atoms, which interfered with the determination of its location in the $F_o - F_c$ omit map. Thus, the position of O5 was determined from the $2F_o - F_c$ map. The average *B*-factor of the five metal ions refined without restrain was 25.3 $Å^2$, which was lower than that of the overall average *B*-factor, of 35.2 $Å^2$ (Supplementary Table 1).

Chloride and metal ions. The existence of two Cl^- ions in the vicinity of the oxygen-evolving complex was previously reported with Br^-- or I^--substituted PSII[26,27]. We confirmed the positions of the two Cl^--binding sites in native PSII both with an $F_o - F_c$ omit map taken at a wavelength of 0.9 Å and analysed to a resolution of 1.9 Å, and with an anomalous difference Fourier map taken at a wavelength of 1.75 Å and analysed to a resolution of 2.5 Å. Several additional calcium and magnesium ions were identified by these two electron density maps, and their structures were constructed by taking their coordination environments into consideration.

Chlorophyll *a* and pheophytin molecules. Electron density distributions for the magnesium atoms of chlorophyll *a* were clearly separated from those for the chlorin rings and were located out of the ring planes in most cases. The chlorin rings were bent to various degrees depending on their environments. The conformations of ethyl and vinyl groups were determined unambiguously from the corresponding electron density distributions. Two optically active centres (C8 and C13) of all of the phytol chains were also recognized as being in the (*R*, *R*) configuration from the electron density map.

Plastoquinones. Two plastoquinones, Q_A and Q_B, were identified from the electron density map, whereas a third plastoquinone, Q_C, reported in a previous structure[5], was not observed. Q_A had a well-defined electron density distribution, resulting in a low average *B*-factor of 25.5 $Å^2$, whereas the electron density for Q_B was weak, resulting in a higher *B*-factor of 76.8 $Å^2$.

Lipids and unknown molecules. Two kinds of lipid molecule, SQDG and phosphatidylglycerol, contained sulphur and phosphorous atoms, respectively, which have larger anomalous dispersion effects at a longer wavelength. The positions of four of eight SQDG molecules and eight of ten phosphatidylglycerol molecules in the PSII dimer were confirmed from the anomalous dispersion of the sulphur and phosphate atoms contained in these lipids, on the basis of the anomalous difference Fourier map calculated from the data set taken at a wavelength of 1.75 Å. The electron densities for a typical SQDG and phosphatidylglycerol are depicted in Supplementary Fig. 2. Other lipid molecules were found and modelled on the basis of the $F_o - F_c$ omit map and the $2F_o - F_c$ map. Six lipids with two fatty-acid chains were found in the dimer, but their species could not be identified. Additionally, 30 single alkyl chains of unknown identity were observed in the dimer; of these, 23 were located adjacently. Therefore, the total number of lipids should exceed 23 in each monomer.

Water molecules. Water molecules were assigned from the $2F_o - F_c$ electron density map at over the 1σ level. Around 1,300 water molecules were found in each monomer (Supplementary Table 1), and a few of them were found to be disordered.

Error estimation for atomic coordinates. The coordinate error was estimated with the diffraction-component precision index (DPI) introduced by Cruikshank[34,40], using the software SFCHECK in the CCP4 suite[38]. The DPI value of the whole PSII structure was found to be 0.11 Å, resulting in a standard uncertainty in the bond length of 0.16 Å.

35. Kabsch, W. Automatic processing of rotation diffraction data from crystals of initially unknown symmetry and cell constants. *J. Appl. Crystallogr.* **26,** 795–800 (1993).
36. Otwinowski, Z. & Minor, M. Processing of X-ray diffraction data collected in oscillation mode. *Methods Enzymol.* **276,** 307–326 (1997).
37. Brünger, A. T. *et al.* Crystallography & NMR system: a new software suite for macromolecular structure determination. *Acta Crystallogr. D* **54,** 905–921 (1998).
38. Collaborative Computational Project, Number 4. The *CCP4* suite: programs for protein crystallography. *Acta Crystallogr. D* **50,** 760–763 (1994).
39. Emsley, P., Lohkamp, B., Scott, W. G. & Cowtan, K. Features and development of Coot. *Acta Crystallogr. D* **66,** 486–501 (2010).
40. Daopin, S., Davies, D. R., Schlunegger, M. P. & Grütter, M. G. Comparison of two crystal structures of TGF-β2: the accuracy of refined protein structures. *Acta Crystallogr. D* **50,** 85–92 (1994).